

## Analysis of cracks and coating in iron ore pellets by digital image processing

<http://dx.doi.org/10.1590/0370-44672019730128>

**Thalita Dias Pinheiro Caldas**<sup>1,3</sup>

<https://orcid.org/0000-0002-7425-3276>

**Karen Soares Augusto**<sup>1,4</sup>

<https://orcid.org/0000-0002-0116-4993>

**Julio César Álvarez Iglesias**<sup>1,5</sup>

<https://orcid.org/0000-0001-7966-6451>

**Sidnei Paciornik**<sup>1,6</sup>

<https://orcid.org/0000-0001-6520-2007>

**Alei Leite Alcântara Domingues**<sup>2,7</sup>

<https://orcid.org/0000-0002-5729-2329>

<sup>1</sup>Pontifícia Universidade Católica do Rio de Janeiro - PUC-Rio, Departamento de Engenharia Química e de Materiais, Rio de Janeiro - Rio de Janeiro - Brasil.

<sup>2</sup>Vale - Centro de Tecnologia de Ferrosos, Belo Horizonte - Minas Gerais - Brasil.

E-mails: <sup>3</sup>[yeshuathalita@gmail.com](mailto:yeshuathalita@gmail.com),

<sup>4</sup>[saugustokaren@gmail.com](mailto:saugustokaren@gmail.com),

<sup>5</sup>[juliooc.alvarez@gmail.com](mailto:juliooc.alvarez@gmail.com), <sup>6</sup>[sidnei@puc-rio.br](mailto:sidnei@puc-rio.br),

<sup>7</sup>[alei.domingues@vale.com](mailto:alei.domingues@vale.com)

### Abstract

The pelletizing process agglomerates ore fines previously considered as tailings and makes its application possible in the form of pellets. During the process, the pellets are subjected to various compressive forces and temperature changes, which cause ruptures in their surface. These ruptures (cracks) impair the performance of the pellets in the reduction furnaces and affect their strength. In addition to cracking, the formation of clusters inside the furnaces is also a problem for the reduction process because they compromise the flow of gases inside the furnaces. This bonding phenomenon occurs from the formation of iron bridges between pellets subjected to high temperatures. This problem can be minimized by coating the pellets with a mixture of magnesium oxides that inhibits bridging. The present study considered the importance of characterizing cracks and coating on the pellet surface and developed methodologies for the acquisition, processing and digital analysis of images acquired with a stereoscope. Adjustable sample holders were developed which made it possible to cover most of the surface area of the spherical object avoiding overlapping of analysis regions. The crack analysis routine used semantic segmentation and provided attributes such as mean thickness, area fraction and length. The coating analysis routine used color threshold segmentation and measured the fraction of the area occupied by the coating in the samples. The use of the sample holders was essential for the success of the acquisition procedure. The analysis routines were robust for different samples.

**Keywords:** iron ore pellets; image analysis; cracks, coating.

### 1. Introduction

Iron ore is an essential raw material in the steel industry, but it must first go through a beneficiation process, which mainly aims at separating valuable minerals from gangue minerals. The beneficiation products are granulated ore, sinter feed and pellet feed, which are essentially differentiated by their particle size.

Unlike granulated ore, sinter feed and pellet feed cannot be used directly in steel mills, so they are subjected to agglomeration processes: sintering and pelletizing, which give rise respectively to sinter and pellets.

The pelletizing process, for example, agglomerates fines with particle sizes below 0.15 mm, forming irregular spheres (pellets) that can be used in reduction furnaces. The pellets have a

diameter in the range of 9-15 mm, high and uniform porosity and an iron content greater than 63% (Meyer, 1980). During the pelletizing process, the pellets undergo a thermal treatment so that they can acquire the necessary strength to withstand severe handling and transport conditions, as well as possible degradation effects during their application in the furnaces (Simões *et al.*, 2015). However, thermally or mechanically induced stresses can give rise to cracking, both internally and at the surface, which compromise the quality of the pellets in their use. In previous studies, Nunes *et al.* (2012) associated the presence of cracks to the reduction of pellet strength.

Besides crack formation, there is another factor that compromises the efficiency of the pellets in the furnaces:

the formation of pellet clusters, caused by the formation of iron bridges due to the high temperatures to which the pellets are subjected (Bailon *et al.*, 2011). These clusters can seriously compromise the flow of gases inside the furnaces.

In order to reduce the formation of clusters, producers use a coating composed of a mixture of magnesium oxides that blocks the formation of iron bridges (Alencar *et al.*, 2014). It is known that characterizing cracks and coatings on the surface of iron ore pellets is important for quality control. Although an ideal value for the amount of cracks has not yet been determined for a pellet to have good strength or how much coating needs to be added to the pellet so that clusters do not occur.

Simões *et al.* (2014) and Simões *et*

al. (2015) used digital image processing to perform this characterization and obtained significant results. When analyzing crack images, for example, it was possible to associate their sizes and widths to the pellet's mechanical performance. In relation to the coating, it was shown that its absence is directly linked to the tendency of cluster formation. However, in these articles, a limited fraction of each surface of the sediment

## 2. Materials and methods

### 2.1 Samples

The samples used in this study were iron ore pellets supplied by Vale. The granules range in diameter from 12 mm to 18 mm. In this procedure, 6 pellets contain-

### 2.2 Image acquisition

One of the main challenges in the image acquisition step was to represent the surface of an irregular spheroid with 2D images, while covering the vast majority of the relevant area. Moreover, it was crucial to guarantee that the various 2D images did not overlap, in order to avoid measurement errors.

Given the typical size of the pellets and the required resolution, the ideal image acquisition apparatus was a stereoscope.

was imaged and analyzed.

Thus, herein, a new image acquisition procedure is proposed so that the vast majority of the pellet surface is covered, leading to more representative results. Moreover, two fully automatic image processing and analysis routines were developed to automatically identify cracks and coating on the surface of the pellets, and measure several relevant parameters, such as coating/crack area

ing cracks (PT) and 4 pellets with coating (PC) were used. This number of samples was used for the development of the methodologies. However, characterization can be per-

This type of equipment seldom has a motorized sample holder and manual handling of the pellet would be necessary. In order to simplify the acquisition procedure a cuboidal sample holder was developed (Figure 1).

The main idea of the cube is to delimit capture areas and standardize so that each pellet sample will always work with six images referring to the six faces of the cube. Importantly, the developed sample holder provide stability during image acquisition

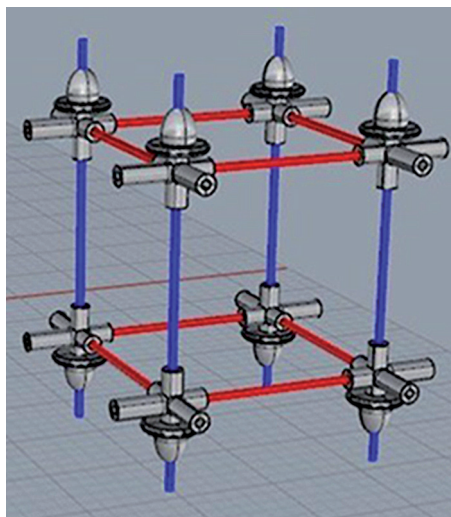


Figure 1 - Support developed for iron ore pellet imaging.

The images were acquired on a ZEISS Discovery V8 stereoscope using a 0.3X objective lens, leading to 1.6X magnification and a digital resolution of 15.49  $\mu\text{m}/\text{pixel}$ . To improve lighting

stability, which is crucial for the image processing routines, a LED ring fixed around the objective lens was used with constant maximum intensity.

Each pellet was inserted in the cube,

fraction, crack length and thickness.

It is expected that a more efficient and representative evaluation of these two features – cracks and coating – will allow an optimization of process parameters. For instance, changes in heat treatment temperature profiles can improve strength by reducing heat-induced cracks. Likewise, changes in the amount and type of coating can be shown to reduce the formation of iron bridges.

formed for a much larger number of samples. It is worth mentioning that the samples were chosen to ensure a good representation of both crack sizes and coating quantity.

and be adaptable to the various pellet diameters. Given these requirements, the sample holder was designed as shown the Figure 1.

The pieces representing the cube vertices were made of silver and with a 0.6 mm opening to allow the edges, which are 0.5 mm thick metal pins, to be fitted, as thin as possible to reduce the loss of area. Four of the edges are movable (in blue in Figure 1), and can be adjusted according to the sample to be analyzed.

## 3. Results and discussion

After image acquisition, processing routines were developed for each

case: cracks and coating. The routines will be presented in this section along

which was then manually positioned and rotated so that each face was imaged.

FIJI/ImageJ (Rueden *et al.*, 2017) was used to develop the image processing and analysis routines.

with the results of the measurements obtained.

### 3.1 Cracks

#### 3.1.1 Obtaining the analysis area

Image acquisition results in six images from each pellet. Figure 2a shows an example of a sample image, PT2, in which it is possible to observe the support delimiting the area to be analyzed, which in this case, would be precisely the square where the largest crack is contained.

The first part of the cracking routine seeks to remove the sample holder from the images so that it is possible to work only with the analysis areas of each cube

face, which will hereafter be referred to as the pellet face. We will use the image of a PT2 pellet face to exemplify the image processing/analysis routine.

Initially, the acquired color images are converted to 8-bits and then segmented with a (0-109) threshold range. Thus, pixels in this tonal range turn white and the remainder appears in black in the binary image, as shown in Figure 2b.

Then the empty spaces are filled giving rise to the image presented in Figure 2c, which is not yet the desired mask, as it contains objects corresponding to the support, and regions belonging to the other faces of the pellet, which would compromise the desired measurements. Then, an area measurement of all the objects in the image is performed, and only the largest area is chosen, such as the one shown in Figure 2d.

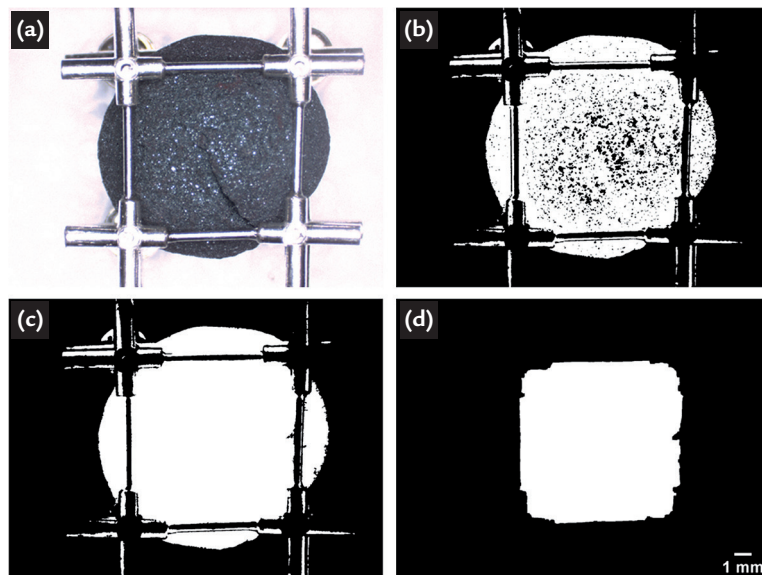


Figure 2 - Schematic representation of the initial part of the processing performed by the routine, using an image of PT2 sample. a) Original image of one face of PT2. b) Binary image after threshold in (a). c) Binary mask after fill holes. d) Mask generated for the analysis area.

Upon obtaining the mask a logical operation is performed pixel by pixel be-

tween the original image (Figure 2a) and the generated mask (Figure 2d), obtain-

ing the images of the respective areas of analysis, as presented in Figure 3.

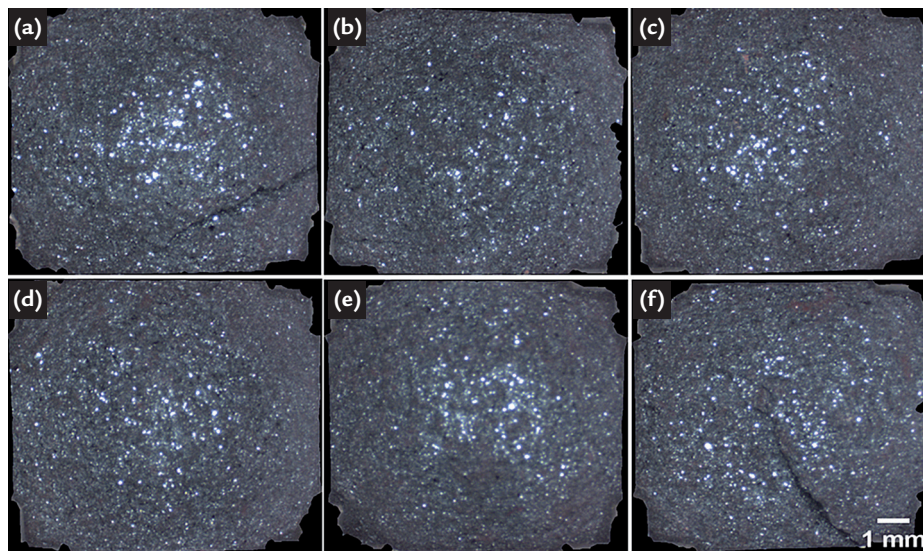


Figure 3 - PT2 sample faces after holder removal.

Given the acquisition of 6 im-

ages corresponding to the faces to be analyzed, the routine moves on to the segmentation part.

### 3.1.2 Segmentation

In this step, the cracks must be selected for subsequent measurement. Crack detection was performed with the WEKA FIJI plugin. According to Arganda-Carreras *et al.* (2017) and Hall *et al.* (2009), tools available in WEKA can extract various properties of the images using pixels that the user himself selects and uses in training. After training several images, the user can create a classifier and apply it to several similar images.

This form of segmentation, called

semantic segmentation, has played an essential role in the area of digital image analysis, and can be described as a way of separating the pixels of an image into classes according to the pixel characteristics of an image, which are reported to the computer through training (Lateef and Ruichek, 2019; Niemeijer *et al.*, 2017).

In FIJI, WEKA can be used directly through a plugin, Trainable Weka Segmentation (TWS). Therefore, from the 36 images referring to the faces of the six PT

samples used, 15 images were chosen that contained a good representation of cracks to perform a training. This is achieved by selecting small areas in each of the images, separating them into two classes: cracks and pellet.

From 584555 selected pixels referring to both classes, a classifier was trained and applied to the images generating results where the cracks appear discriminated from the rest of the pellet, as can be seen in Figure 4b.

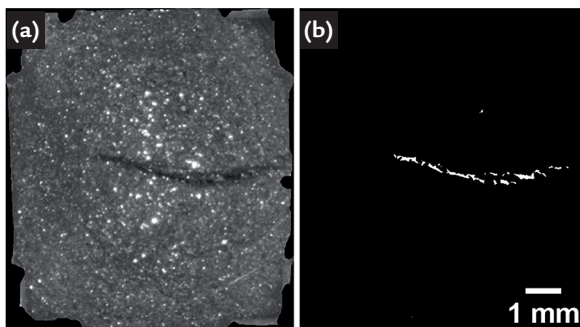


Figure 4 - Images of cracks on a PT2 face.

a) Original image 8-bit. b) Binary image with crack selected from classifier.

The created classifier was then applied to the 36 face images of the PT samples. Analyzing the results, it can

be seen that the classifier differentiates the crack well from the rest of the pellet, with the exception of very narrow

cracked areas, as shown in Figure 5 in which the crack is narrower.

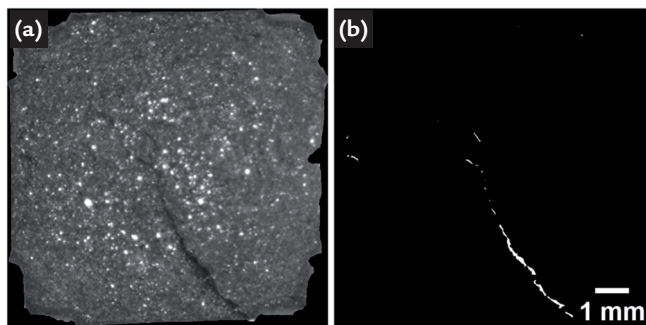


Figure 5 - Images of thinner cracks on a PT2 face.

a) Original image 8-bit. b) Binary image with crack selected from classifier.

The difficulty of selecting narrow areas during training comes from assigning classes of the marked area,

since it is necessary to closely zoom in on the image, whereby the resolution is compromised, making it difficult

to differentiate pixels from these very narrow cracks.

### 3.1.3 Attribute extraction

From the binary image containing the cracks, a post-processing is performed in order to connect objects belonging to the cracks. This consisted of a morphological closing (Legland *et*

*al.*, 2016) operation using an octagonal Structuring Element (EE).

After the objects are joined, spurious objects are eliminated by the area value. The set value has been tested

on many images to ensure that no objects belonging to the cracks have been deleted. Figure 6 shows this post processing performed on one side of the PT4 sample.

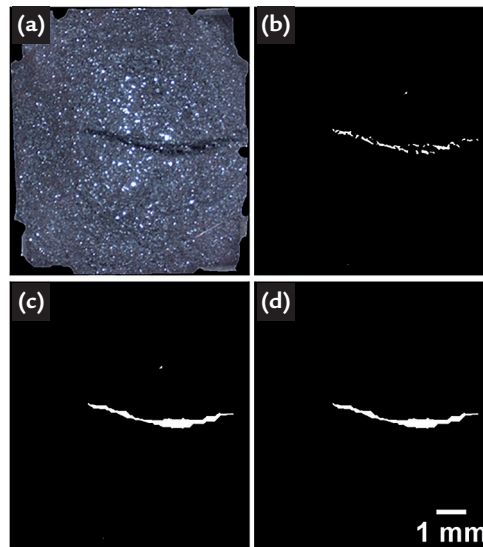


Figure 6 - Segmentation of cracks in one face of PT4. a) Original image  
 b) Binary image with crack selected from classifier. c) Binary image after post processing, still containing spurious objects. d) Binary image containing the crack after the exclusion of spurious objects.

From the post-processed image, crack area and perimeter measurements

are performed. These values make it possible to calculate length using the formula:

$$Length = \frac{PERIM + \sqrt{(PERIM)^2 - 16 \cdot AREA}}{4}$$

This parameter, also known as Fiber Length, is more accurate than the more straightforward measurement of the Maximum Feret (Caliper) if the object is curved (Vameraliv *et al.*, 2003). For instance, the crack presented in Figure 6d is 5.23 mm in length, but its Maximum Feret is 4.87 mm.

In some samples one cannot merge all crack objects into one. If the value of the morphological closing is too high, it is

possible to include objects that one does not want to measure. Therefore, the length is calculated for each object and then summed, thus obtaining a total length for each face of the sample.

The morphological operation is only used to eliminate smaller objects and join objects that belong to the crack. As the operation increases the size of objects, to perform the other measurements, an intersection is made between the generated

image of the classifier (Figure 6b) and the post processed image (Figure 6d), obtaining the image shown in Figure 7a. This is the reference image for the next step, that involves thickness measurements. Although the object in Figure 6d gives a better assessment of the crack total length, the thickness is clearly overestimated. Using Figure 7a for thickness measurement, as explained in the following, gives a more representative result.

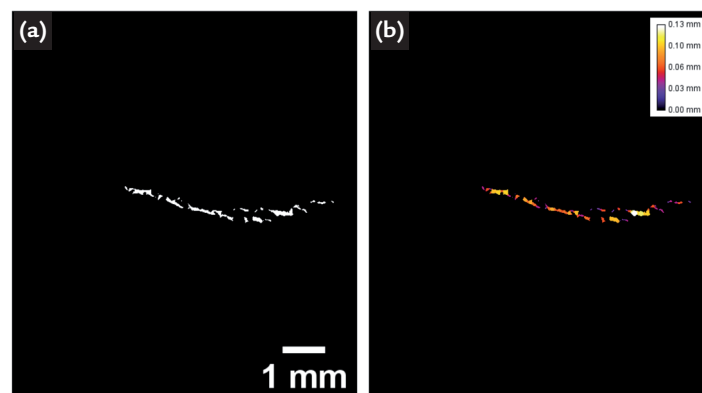


Figure 7 - Cracked image of one face of PT4. a) Post-processing image containing only the crack. b) Local thickness map of the crack contained in (a), with a color LUT to improve visibility.

The local thickness map assigns different intensities to each pixel belonging to the objects. The local thickness of each point in the image is defined by the diameter of the largest sphere inside the object that contains the point (Dougherty and Kunzelmann, 2007).

Figure 7b displays the local thickness map for one face of PT4, with a color Look Up Table (LUT) to improve visibility. Thus, for each crack, it is possible to obtain a local thickness for every position along the crack length and, thus, an average thickness for each crack. Through the

arithmetic mean of all crack values of each sample, it is possible to obtain the average thickness for each PT sample. In the case of the sample to which this face belongs, the average thickness is 0.046 mm.

This approach is much more flexible than other methods that rely on

measuring line intercepts, for instance, as it is totally independent of object shape or orientation. It is also worth mentioning that, even though the object shown in Figure 7a is discontinuous, the estimate of average thickness is reason-

able exactly because the “missing” segments are the thinnest. As mentioned above, this would not be the case, if the thickness were measured on the object in Figure 6d.

The crack area fraction can also be

easily obtained dividing the total crack area in each face by the corresponding face area (Figure 2d) and adding for the 6 faces. Table 1 presents the area fraction values for each of the 6 samples used in this study.

Table 1 - Crack area fractions in each sample PT.

Sample	Area Fraction (%)
PT1	0.091
PT2	0.080
PT3	0.135
PT4	0.088
PT5	0.128
PT6	0.065

The measurements were considered consistent with what can be visually ob-

served in the images. Samples PT3 and PT5 are indeed the ones with larger and

thicker cracks, thus occupying an area fraction slightly larger than the others.

### 3.2 Coating analysis

The same procedure described in Section 3.1.1 to obtain the analysis area

was used in this case. Figure 8 shows a typical image of a coated pellet. The

coated areas appear in hues close to red/orange.

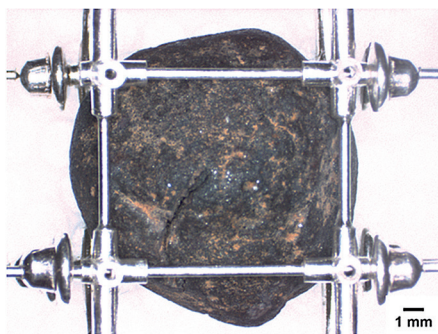


Figure 8 - Coated iron ore pellet sample.

Segmentation was performed in the Hue, Saturation, Brightness (HSB) color space (Ferreira and Rasband, 2012). By

selecting the appropriate hue range, representing colors close to Red, and adjusting for variations using the two other chan-

nels, coating segmentation was successful, as shown in Figure 9, and adapted well to variations between the samples.

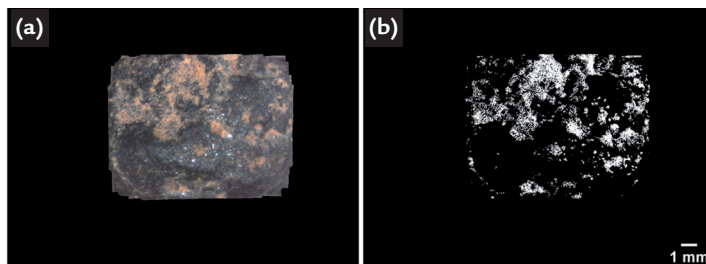


Figure 9- Coated iron ore pellet face.

a) Original image of the analysis area. b) Binary image containing only the coated area.

A problem with most pellet faces is the presence of bright spots from the incidence of light on the uneven surface, visible in Figure 9a. Often these points are not part of the coated area and it is difficult to make this separation. Color segmentation was

also able to deal with this problem.

After eliminating small spurious objects (Figure 9b), the area fraction of coating was obtained summing the coated area in all 6 faces and dividing this by the total area of all faces.

Table 2 shows the area fraction

values for the PC samples. The wide variation in coating area fraction is consistent with semi-quantitative analyses performed visually, and is linked to the coating process uniformity, adhesion, among other variables.

Table 2 - Area fractions occupied by coating on PC samples.

Sample	Area Fraction (%)
PC1	10.37
PC2	19.48
PC3	2.03
PC4	12.68

#### 4. Conclusions

The present study aimed to develop a methodology for the acquisition of 2D images of the external surface of spheroidal iron ore pellets. For this challenge, cube-shaped supports were developed to allow for stable and reproducible image acquisition conditions. Thus, the spheroidal surface was represented by 6 images corresponding to the 6 faces of the holder, which allowed the delimitation of the capture areas while avoiding superposition between images. The use of the holder also prevented the repetition of regions and provided stability to the spherical objects, besides being adjustable to possible variations of pellet diameter. Given the large depth of focus of the stereoscope used, the images preserved good enough sharpness even at the edges of the field.

Two image processing and analysis routines were developed for the identification and quantification of cracks and coating on the pellet surface.

The crack analysis routine used semantic segmentation based on supervised classification and proved viable for most cases. The main limitation was very narrow cracks that were not accurately segmented. As a possible improvement, an increase in the training data set to include narrow cracks is envisaged. Another possibility is the use of Deep Learning, a technique that has shown excellent results where more traditional approaches have failed (Iglesias *et al.*, 2019).

The coating analysis routine used color segmentation and was shown to be robust for the tested pellets. However,

this approach is likely to be sensitive to illumination conditions and requires a stable source of illumination with constant brightness and color distribution, such as that which is obtained with LED sources.

The developed routines will be used routinely in the labs of the Ferrous Technology Center of Vale, where their robustness will be further tested. The results obtained will allow a quantitative study of the correlation between the number of cracks and the mechanical strength of the pellets, as well as between the amount of coating with the formation of pellets clusters. In turn, this can allow the determination of optimal processing parameters for the several pelletizing steps.

#### Acknowledgements

The financial support of Brazilian funding agencies CNPq, CAPES and

FAPERJ is gratefully acknowledged. The technical expertise of Natascha Scagliusi

was fundamental in the development of the sample holder.

#### References

- ALENCAR, J.; EMRICH, M.; DOMINGUES, A. Study of alternative coating to high temperatures of bustle gas. *In: SEMINÁRIO DE REDUÇÃO DE MINÉRIO DE FERRO E MATÉRIAS-PRIMAS*, 44., 2014, Belo Horizonte. *Anais [...]*. Belo Horizonte: [s.n], 2014. p. 1-13.
- ARGANDA-CARRERAS, I.; KAYNING, V.; RUEDEN, C.; ELICEIRI, K. W.; SCHINDELIN, J; CARDONA, A.; SEUNG, H. S. Trainable Weka Segmentation: a machine learning tool for microscopy image segmentation. *Bioinformatics*, [S.l.], v.33, n. 15, p. 2424-2426, mar 30, 2017.
- BAILON, A. M. G.; SIMÕES, H. O.; BUENO, P. G.; PEREIRA, J. G.; DOELLINGER, T. M.; BIANCHI, M. R. R. Determination of a methodology to evaluate the causes of clustering formation in direct reduction reactors. *In: SEMINÁRIO DE REDUÇÃO DE MINÉRIO DE FERRO E MATÉRIAS-PRIMAS*, 41.; SEMINÁRIO BRASILEIRO DE MINÉRIO DE FERRO, 12., 2011, Vila Velha. *Anais [...]*. Vila Velha: [s.n], 2011. p. 1152-1159.
- DOUGHERTY, R.; KUNZELMANN, K. Computing local thickness of 3D structures with ImageJ. *Microscopy and Microanalysis*, v. 13, n. S02, p.1678-1679, 2007.
- FERREIRA, T.; RASBAND, W. *ImageJ User Guide*. [S.l.: s.n], 2012. Available at: <http://fiji.sc/guide.git>.
- HALL, M.; FRANK, E.; HOLMES, G.; PFAHRINGER, B.; REUTEMANN, P.; WITTEN, I. H. The WEKA Data Mining Software: an update mark. *Children's Geographies*, [S.l.], v. 11, n. 1, p.10-18, may 2, 2009.
- IGLESIAS, J. C. Á.; SANTOS, R. B. M.; PACIORNIK, S. Deep learning discrimination of quartz and resin in optical microscopy images of minerals. *Minerals Engineering*. [S.l.], v. 138, p. 79-85, may 6, 2019.
- LATEEF, F.; RUICHEK, Y. Survey on semantic segmentation using deep learning techniques. *Neurocomputing*, v. 338, p. 321-348, 2019.
- LEGLAND, D.; ARGANDA-CARRERAS, I.; ANDREY, P. MorphoLibJ: integrated library and plugins for mathematical morphology with ImageJ. *Bioinformatics*, v. 32, n.22, p. 3532-3534, 15 nov. 2016. DOI: <https://doi.org/10.1093/bioinformatics/btw413>.
- MEYER, K. *Pelletizing of iron ores*. New York: Springer-Verlag, 1980.

- NIEMEIJER, J.; FOUOPI, P. P.; BARTH, E. A Review of neural network based semantic segmentation for scene understanding in context of the self driving car. *Bioinformatics*, [S.l.], p.1-4, ap 11, 2017.
- NUNES, R. A. P.; RODRIGUES, E. S.; ALVES, F. Study of cracks in iron ore pellets. In: SEMINÁRIO DE REDUÇÃO DE MINÉRIO DE FERRO, 47., 2012, São Paulo. *Anais* [...]. São Paulo: [s.n.], 2017. p.82-89.
- RUEDEN, C. T. *et al.* ImageJ2: ImageJ for the next generation of scientific image data. *BMC Bioinformatics*, v. 18 , n. 529, nov. 2017. DOI 10.1186/s12859-017-1934-z. Available at: <https://fiji.sc/>. Accessed: jul 13, 2019.
- SIMÕES, H. O. O.; BAILON, A. M. G.; SILVA, R. R. A.; MESCHIATTI, A.; PASSIGATTI, V. P.; DOELLINGER, T. M. Development of a methodology for determining the percentage of coating around the pellet by automatic image analysis. In: CONFERENCIA DEL ACERO IAS, 20., 2014, Rosario. *Anales* [...] Rosario: [s.n.], 2014. p.649-661.
- SIMÕES, H. O.; BAILON, A. M. G.; MESCHIATTI, A.; SILVA, R. R. A.; PASSIGATTI, V. P.; FONSECA, M. C. Creating algorithm for analysis of broken images and burned pellet and correlation of its parameters with the physical strength of the material. In: SEMINÁRIO DE REDUÇÃO DE MINÉRIO DE FERRO E MATERIAIS-PRIMAS, 45., 2015. *Anais* [...]. Rio de Janeiro: [s.n.], 2015. p. 961-969.
- VAMERALI, T. *et al.* Analysis of root images from auger sampling with a fast procedure: a case of application to sugar beet. *Plant and Soil*, v. 255, n. 1, p. 387-397, 2003.

---

Received: 10 September 2019 - Accepted: 3 March 2020.